Journal of The
Electrochemical Society

Wet-Chemical Synthesis of a Protective Coating on NCM111 Cathode: The Quantified Effects of Washing, Sintering and Coating

To cite this article: Liga Maskova *et al* 2024 *J. Electrochem. Soc.* **171** 100520

Journal of The Electrochemical Society, 2024 **171** 100520

Wet-Chemical Synthesis of a Protective Coating on NCM111 Cathode: The Quantified Effects of Washing, Sintering and Coating

Liga Maskova,[1,2] Reinis Ignatans,[1] Arturs Viksna,[3] Anatolijs Sarakovskis,[1] Maris Knite,[2] and Gints Kucinskis[1,z]

[1]*Institute of Solid State Physics, University of Latvia, Riga, LV-1063, Latvia*
[2]*Faculty of Natural Sciences and Technology, Riga Technical University, Riga, LV-1048, Latvia*
[3]*Department of Analytical Chemistry, Faculty of Medicine and Life Sciences, University of Latvia, Riga, LV-1004, Latvia*

$LiNi_xCo_yMn_{1-x-y}O_2$ (NCM) cathodes, especially with high Ni content, are widely expected to keep advancing the energy density of Li-ion batteries. However, ensuring a good cycle life remains a key challenge. Applying inert protective coatings on the surface of NCMs is a common route for mitigating surface-based degradation. In this study a sustainable ethanol-based wet-chemical coating method for covering the material with Al_2O_3 is developed and demonstrated on NCM111. The effect of the synthesis procedure is carefully evaluated to distinguish the benefits of the protective coating from the contributions of re-sintering and removal of surface contaminants, all taking place during the synthesis of the coated material. We show that while the cycling stability is significantly improved by the material regeneration alone (65% vs 79% state-of-health after 500 charge-discharge cycles at voltage range 2.7–4.3 V vs Li/Li^+), the Al_2O_3-coated material displays further cycle life gains, maintaining 88% of initial capacity after 500 charge-discharge cycles. This work thus demonstrates both a sustainable wet-chemical coating method and the importance of establishing a proper baseline for characterization of inert protective coatings in general. The importance of both gains further prominence with the transition to inherently less stable higher Ni content NCMs.
 [DOI: 10.1149/1945-7111/ad8483]

Manuscript submitted August 7, 2024; revised manuscript received September 24, 2024. Published October 17, 2024.

Supplementary material for this article is available online

Lithium-ion batteries (LIBs) are among the leading energy storage technologies. The active anode and cathode materials used in LIBs have a disproportionately large impact on the performance of the battery and are thus a subject of continuous research.[1] On the forefront of the cathode development are $LiNi_xCo_yMn_{1-x-y}O_2$ (NCM) layered transition metal oxide materials. To increase the specific energy of NCM and minimize the use of cobalt, a critical raw material, a key research focus has been on increasing the amount of nickel–from NCM111 to the current state-of-art NCM811 (numbers denote the stoichiometric ratio between Ni, Co, and Mn), to Ni-rich NCM materials with ever higher Ni content. While Ni-rich materials have some of the highest energy densities among Li-ion battery cathodes, as the amount of Ni is increased, and Co content lowered, the thermal, structural, and cycling stabilities deteriorate.[2]

The degradation processes typically plaguing NCM cathodes during battery operation are cation mixing, oxygen evolution, side-reactions with the electrolyte, and cathode-electrolyte interphase (CEI) growth, with all intensifying as the Ni content increases.[3] Additionally, surface impurities, such as residual lithium compounds (RLCs) and transition metal (TM) carbonates (mainly $NiCO_3{\cdot}2Ni(OH)_2{\cdot}xH_2O$)[4] form on NCM cathode materials during synthesis and storage. Besides being dead weight, the presence of RLCs and TM carbonates is also detrimental to electrode preparation and battery operation.[3–5] Thus, strategies to minimize the amount of lithium and transition metal species on the surface of NCMs are needed.

Our meta-analysis shows that inert protective coatings synthetically formed on active material particles helps to prevent cycling ageing of NCM materials, with protective coatings having an outsized impact on the capacity retention of NCM111.[3] Furthermore, the benefits of the inert protective coatings are still retained with increasing Ni content (NCM811 and beyond),[6–8] as surface-based degradation is exacerbated with increased Ni content. The protective coatings on cathode particles or on whole electrodes can mitigate side-reactions with the electrolyte, hinder oxygen and TM dissolution from the cathode material, scavenge HF formed due to electrolyte decomposition, and at times improve electronic (carbon-based coatings,[9,10] conductive polymer coatings[7,11]) or ionic (Li_3PO_4,[12] LiF,[13] Li_3VO_4[14]) conductivity. As a result, the cycle life of the battery is extended. For most coatings the thickness should be strictly limited to prevent an increase in electrochemically inactive mass and thus loss of gravimetric capacity. The thickness of non-conductive coatings should also be controlled to avoid an increase in internal resistance.

Atomic layer deposition (ALD) and chemical vapor deposition (CVD) are typically used in scientific literature and enable accurate control of the thickness and uniformity of the coatings. However, while suited for lab-scale development, these methods are time-consuming, costly, and require instrument-specific knowledge and skills for fabrication, thus their application on an industrial scale remains challenging.

For cost and time efficiency one of the preferred synthesis methods is wet chemical coating which usually involves mixing the active material in a solvent, adding the coating precursor, and a concluding sintering step to obtain the final product.[6,15,16]

Our work focuses on the development of a facile, sustainable, ethanol-based wet chemical coating of NCM111 with Al_2O_3. While many studies often employ water,[8,15] toluene[17] or other solvents,[18] ethanol is a sustainable alternative that allows to forego the challenging aqueous processing and minimizes the risk of loss of lithium.[19] The synthesis employs a surface-based reaction, forming hydrogen bonds between the surface oxygen groups of the layered transition metal oxide particles and hydrolyzed isopropoxide compounds (hydroxides), followed by a subsequent sintering step. Additionally, washing in ethanol has been shown to improve the resistance to moisture and CO_2 in air during subsequent storage.[19,20]

Interestingly, sintering in conditions similar to what are being used in the synthesis of protective coatings has been shown to also improve the electrochemical performance through surface reconstruction and removal of RLCs.[21] If the active material used for coating has not been handled properly at any point during its delivery or processing, the improved cycle life observed due to the

[z]E-mail: gints.kucinskis@cfi.lu.lv

re-sintering and removal of RLCs could be falsely attributed to the protective coating. Indeed, wet chemical coating studies typically focus on the comparison between the pristine and coated material, attributing all the stability and capacity improvements to the developed coating.[6,15,18] The magnitude of the positive effects that washing and sintering have on the active material[22,23] in this type of processing thus remains elusive. To thoroughly evaluate the effect that the inert protective coating has on the active material, in this study, besides contrasting the performance of coated and uncoated materials, we also systematically investigate the effects of the washing and sintering steps on NCM, together and separately. In addition to the electrochemical performance, we also analyze surface chemistry and determine the amount of carbon to quantify the changes in active material composition and subsequent improvements in cycle life to washing, sintering and coating steps.

Experimental

Coating preparation.—Wet-chemical coating synthesis was developed on a commercially sourced pristine NCM111 (MTI Corp.), which had been stored in a vacuum desiccator for approximately a year. Aluminium isopropoxide (AIP) was used as raw material for the coating. The process of the coating synthesis is described below.

1. AIP was dissolved in anhydrous ethanol.
2. NCM111 active material was then added to the mixture so that the weight proportion of Al_2O_3 coating in the final product would be 3%. The mixture was stirred for 30 min at 400 rpm to disperse the materials evenly.
3. A stoichiometric amount of H_2O was then added to react with AIP and form $Al(OH)_3$.
4. The mixture was stirred for 2 h to allow $Al(OH)_3$ coordination around the active material particles.
5. The mixture was subsequently centrifuged and washed with anhydrous ethanol twice to get rid of any uncoordinated $Al(OH)_3$ and other impurities.
6. The remaining slurry was transferred to a crucible and dried at 80 °C overnight.
7. The following day the dried powder was sintered at 500 °C in air for 4 h (heating rate 4 °C min^{-1}) and cooled down to room temperature thereafter.
8. The obtained powder was stored under Ar atmosphere (O_2 and H_2O <0.5 ppm) until further processing.

The reference sample was produced following steps 2.−8. (the exact same procedure, without adding AIP and H_2O as the coating-forming agents). The washed sample was produced following steps 2.−6. (drying in vacuum at step 6), 8. and the sintered sample was produced by following steps 7.−8. A visualization of all sample preparation procedures is depicted in Fig. 1.

Material characterization.—The structure of unmodified (commercially sourced NCM111) and modified (coated, reference, washed, and sintered) NCM111 materials was analyzed by powder X-ray diffraction (XRD) analysis in Rigaku MiniFlex 600 benchtop XRD (Cu $K\alpha_{1,2}$). Rietveld refinement was performed by using Profex 5.2.8 software.

The XPS measurements were carried out using a ThermoFisher ESCALAB Xi+ instrument using a monochromatic Al Kα X-ray source. The calibration of the binding energy scale is confirmed by examining the sputter-cleaned Au, Ag, and Cu reference samples that place Au $4f_{7/2}$, Ag $3d_{5/2}$, and Cu $2p_{3/2}$ peaks at 83.96 eV, 368.21 eV, and 932.62 eV, respectively. The spectra were recorded using an X-ray beam size of 650 × 100 μm with a pass energy of 20 eV and a step size of 0.1 eV. Charge neutralizer was used in the reported experiments. The sample powders were pressed into tablets with 5 mm diameter and stored in an Ar filled glovebox. To minimize the formation of undesired impurities on the surface of the analyzed samples, an inert gas-filled transfer vessel was used to transport the samples from the glovebox to the XPS analysis chamber without exposure to air. Prior to the XPS analysis, the surface of the samples was gently etched in situ using Ar^+ ions. Special care was taken to avoid altering the sample chemistry due to potential preferential sputtering.

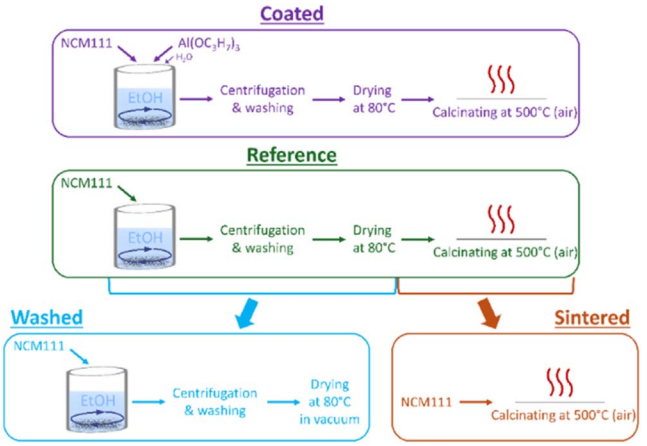

Figure 1. Sample preparation procedures.

The surface morphology was analyzed by scanning electron microscopy (SEM, Thermo Fisher Scientific Helios 5 UX, accelerating voltage 10 kEv) coupled with element distribution analysis (EDS) for powders directly after syntheses. Accelerating voltage applied for EDS measurements was 20 keV.

Transmission electron microscope (TEM, Fei Tecnai running at 200 kV in STEM mode) coupled with EDAX EDS detector was used to ascertain the presence of an Al-containing coating and determine the approximate coating thickness. A lamella was prepared for the STEM analysis from the coated NCM111 powder by depositing a particle on top of a Si wafer, the particle was covered with thick FIB deposited Pt layer for the surface protection. A standard lamella preparation method was employed further (ion beam with 30 kV acceleration voltage was used to thin the lamella to about 100 nm thickness, this was followed by final polishing with 5 kV accelerated ions to reduce the thickness of the amorphized surface layers).

To determine aluminum content in the coated sample, inductively coupled plasma mass spectrometry (8900 ICP-QQQ mass spectrometer, Agilent Technologies, Santa Clara, CA, USA) was used. Quantification of impurities was done using five-point calibration graph method by diluting certified multielement standard solution. For the analysis of carbon traces mainly in the form of surface impurities isotope ratio mass spectrometry (IRMS, Nu Horizon, Wrexham, United Kingdom) coupled with Elemental analyzer (EuroVector Euro EA3000, Pavia, Italy) was used. For the quantification of carbon, a five-point calibration graph was applied using the laboratory reference material (2% C in MnO_2).

Electrode preparation.—Electrode slurries were prepared from all samples by combining the active material with carbon black and PVDF binder in a 75:15:10 ratio in N-methyl-2-pyrrolidone. The slurries were mixed by magnetic stirring at 400 rpm for 2 h, subsequent ultrasonication at 37 kHz for 30 min, and additional stirring at 400 rpm for 30 min. The prepared slurries were manually tape-cast on Al foil with a final wet thickness of 100 μm. The electrode sheets were dried at 80 °C under vacuum overnight. Finally, electrode discs (d = 1 cm) were punched from the electrode sheet for further battery assembly.

Battery cell assembly.—Half-cells with NCM111 electrodes were assembled in an argon-filled glove-box (O_2 and H_2O amount < 0.5 ppm) using grade 316 steel coin cell casings, Whattmann GF/B (Cytiva, Washington, DC, USA) glass fiber separators and 1 M

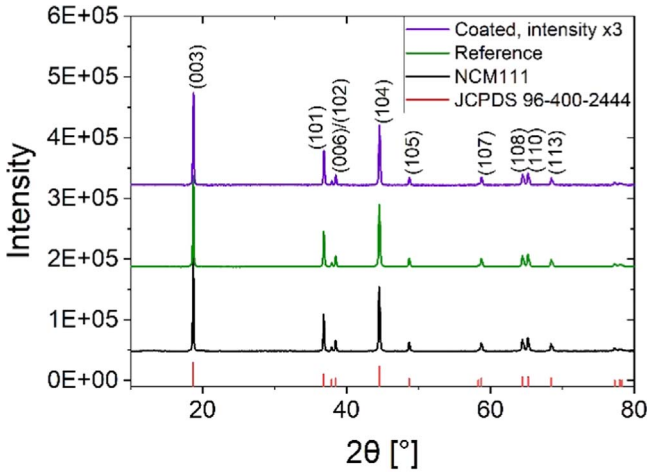

Figure 2. XRD patterns of pristine, reference and coated NCM111. In the reference (green line) and coated (purple line) samples no new phases of Al_2O_3 can be observed in comparison to the pristine NCM111 (black line) indicating that the coating is thin and possibly amorphous.

$LiPF_6$ electrolyte in ethylene carbonate—diethyl carbonate (EC-DEC) mixture with a volume ratio of 1:1 (Sigma Aldrich, battery grade).

Electrochemical characterization.—The assembled half-cells were tested using a Neware BTS-4000 series battery tester at a controlled 25.0±0.1 °C temperature in a constant current (CC) charge and discharge mode. For cycling stability measurements all half cells were charged and discharged at 1 C (170 mA g^{-1}) current density for 500 charge-discharge cycles. For rate capability measurements the half cells were charged and discharged in CC mode at current densities ranging from 0.1 C to 20 C.

Results and Discussion

Material characterization.—Washing and sintering of electrode materials are steps which are included in all wet-chemical coating syntheses. Usually, the coating precursor is mixed with the electrode active material in a suspension, after which the suspension is dried and sintered. The coated material is then contrasted with the uncoated material and all improvements to the electrochemical performance are often attributed to the effects of coating. Although properly coating the cathode active materials is very likely to improve the electrochemical performance, a considerable improvement of the electrochemical properties may be achieved by the washing and sintering steps alone, especially if the source material has been improperly stored allowing surface contaminants to form, promoting cation mixing and surface layered-to-spinel phase transition.[22,24,25] Thus, to specifically address the effect of the standalone coating, in this study, the effects of washing and sintering are excluded by contrasting the electrochemical performance of the coated active material with that of the washed and sintered material (reference sample).

Since washing, sintering, and coating modify the surface of the active material, the electrode preparation method must be adapted accordingly, for the effect to be most prominent. Aggressive mixing methods such as wet ball milling or intensive high shear mixing can crush the secondary active material particles, revealing new unmodified surfaces from the particle bulk, thus the improvements of material stability resulting from the surface coating may be obscured by the degradation of the newly exposed uncoated surfaces.[26–29] Furthermore, while the homogeneity of the electrode is improved, destroying the particle integrity by ball milling has been shown to have a negative impact on the electrochemical performance.[30] Thus, we have opted for a relatively mild mixing method of magnetic stirring followed by sonication to retain the particle integrity and ensure electrode homogeneity. This enables a direct comparison between the pristine, coated and reference materials, which might not be possible when using more vigorous and energy-intensive mixing methods.

Examining the XRD results (Fig. 2) of the pristine, reference, and coated NCM111, no new phases can be seen in the modified samples, indicating that the coating is thin and/or amorphous. No changes were observed for the only sintered and only washed samples either. The *a* lattice parameter remains constant when modifying NCM111 (~2.8618 Å) and the *c* lattice parameter (14.2373 Å) shows only a very slight increase in reference and coated materials of less than 0.001 Å. The observed lattice parameters are in good agreement with those reported by others.[31,32] Rietveld refinement results and statistical errors are compiled in supplementary information Fig. S1 and Tables S1–2. An increase in

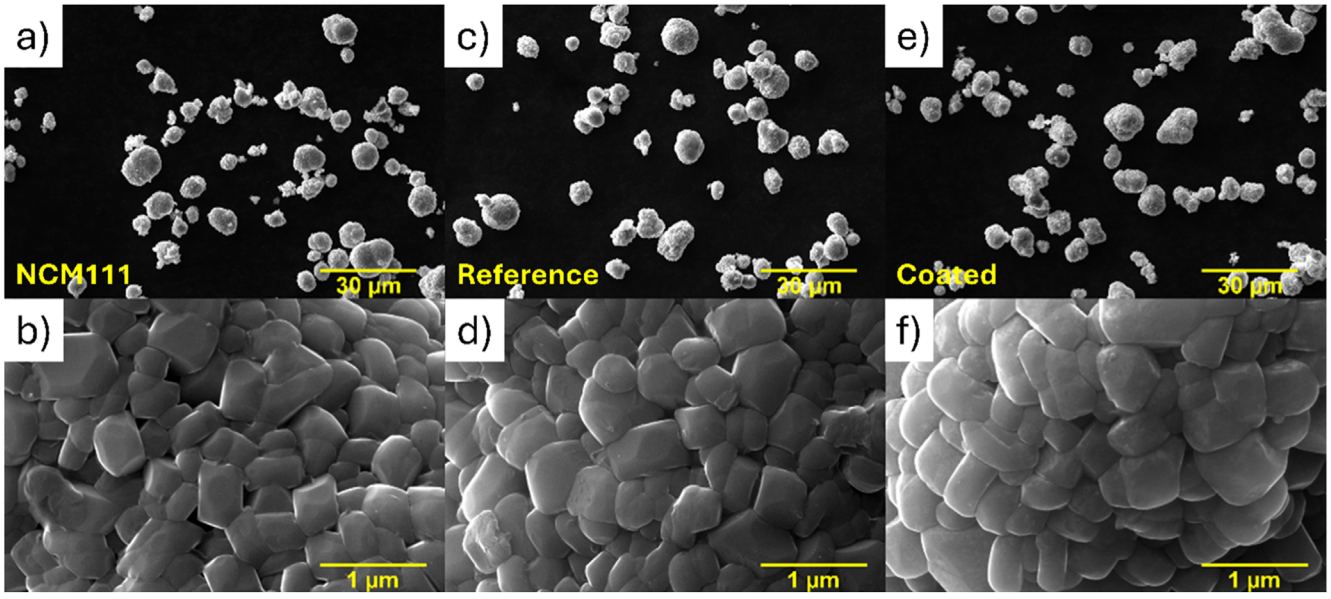

Figure 3. SEM images of pristine (a-b), reference (c-d), and coated (e-f) NCM111. No significant change in particle morphology and size is observed from the low-magnification images (a,c,e). In the higher-magnification image of the coated sample (f) the coating cannot be clearly discerned indicating a very thin layer of coating.

c/a ratio, such as observed here (Table S1), has been linked to improved layered structure and, thus, improved Li^+ diffusivity of NCM cathode materials.[33] Additionally, since Al^{3+} ions have a smaller radius than Ni^{2+} and Li^+ ions, substitution or doping would be seen as a decrease in lattice parameters. Since no decrease is observed, we can conclude that Al^{3+} doping does not take place in the bulk of the coated samples or is so minuscule and surface-based that it cannot be detected by XRD. Absence of Al^{3+} doping is also substantiated in several coating studies where heating even up to 800 °C does not evoke significant Al^{3+} diffusion into the particle due to presence of Mn in the lattice.[15,34,35]

The (003)/(104) peak intensity ratios from XRD patterns are often used as a rule-of-thumb indication of the degree of cation mixing in the active material–values above 1.2 indicate little to no cation mixing. These ratios of the pristine, reference and coated samples are 1.50, 1.47, and 1.55, respectively, showing that cation mixing is not a principal issue in the NCM111 material. Cation mixing determined by Rietveld refinement (Table S1) shows values of around 2% for all samples (all values match within error bounds). Since cobalt in NCM cathodes can stabilize the lattice and mitigate cation mixing,[36,37] cation mixing and its reversal by washing, sintering or coating[38] might become more pronounced in NCMs with higher Ni content.

Based on the SEM images (Fig. 3), washing, sintering or the combination of both do not affect the particle size or surface morphology of NCM111 active material. This suggests that the amount of impurities on the surface of NCM111, which theoretically would be removed in the reference sample, is not significant enough to be visible at this magnification. There is also no thick coating visible on top of the coated NCM111 particles, which is preferred, as the desired thickness of the synthesized coating is in the nanometer scale. Furthermore, the average primary and secondary particle size is not affected by sample modification. The secondary and primary particle distribution of pristine, reference, and coated NCM111 is presented in Fig. S2.

The nanometer-scale coating is revealed by STEM-EDS analysis (Fig. 4). STEM bright field image (Fig. 4a) shows the edge of the secondary particle with a 10 nm thick Al-containing coating. The red line in Fig. 4a represents the location where EDS line spectrum collection was performed (length of line profile was ~ 27 nm, drift corrected spectrum was collected in 27 steps resulting in roughly one spectrum per nm). As seen in EDS line profile Fig. 4b - a drop in Ni, Mn and Co characteristic X-ray counts is observed with a simultaneous increase in Al counts, indicating that the coating is formed right on the surface of the secondary particle. Increase in Al characteristic X-ray counts is observed in ≈ 10–20 nm interval of the line profile, indicating that the coating is about 10 nm thick. Figure 4c represents integrated line profile spectrum clearly showing presence of Al, additionally strong Ga and Pt signals are observed originating from the deposited protective layer.

XPS analysis of the uncoated, reference and coated samples (Fig. 5) reveals changes in their surface chemistry. All samples display characteristic Ni, Co, and Mn peaks of the NCM cathode material (Fig. 5a). Looking closer, only the coated sample clearly shows the band at around 73.2 eV corresponding to $Al_2O_3/LiAlO_2$[39] (Fig. 5d), the intensity of which is reduced as the sample is etched, confirming that Al is largely localized on the surface of the sample. A coating of such chemistry is expected to form during the sintering step of the coating procedure since the lithium from the active material can readily migrate into the Al_2O_3 framework at such high temperatures, forming $LiAlO_2$.[40,41]

The two characteristic XPS peaks in the oxygen binding energy region (Fig. 5c) at 529.5 eV and 531.5 eV corresponding to oxygen in the metal oxide framework of the NCM material and oxygen from the surface impurity species (OH^- and CO_3^{2-}),[42,43] respectively, are clearly distinguishable in all samples. The metal oxide peak of the

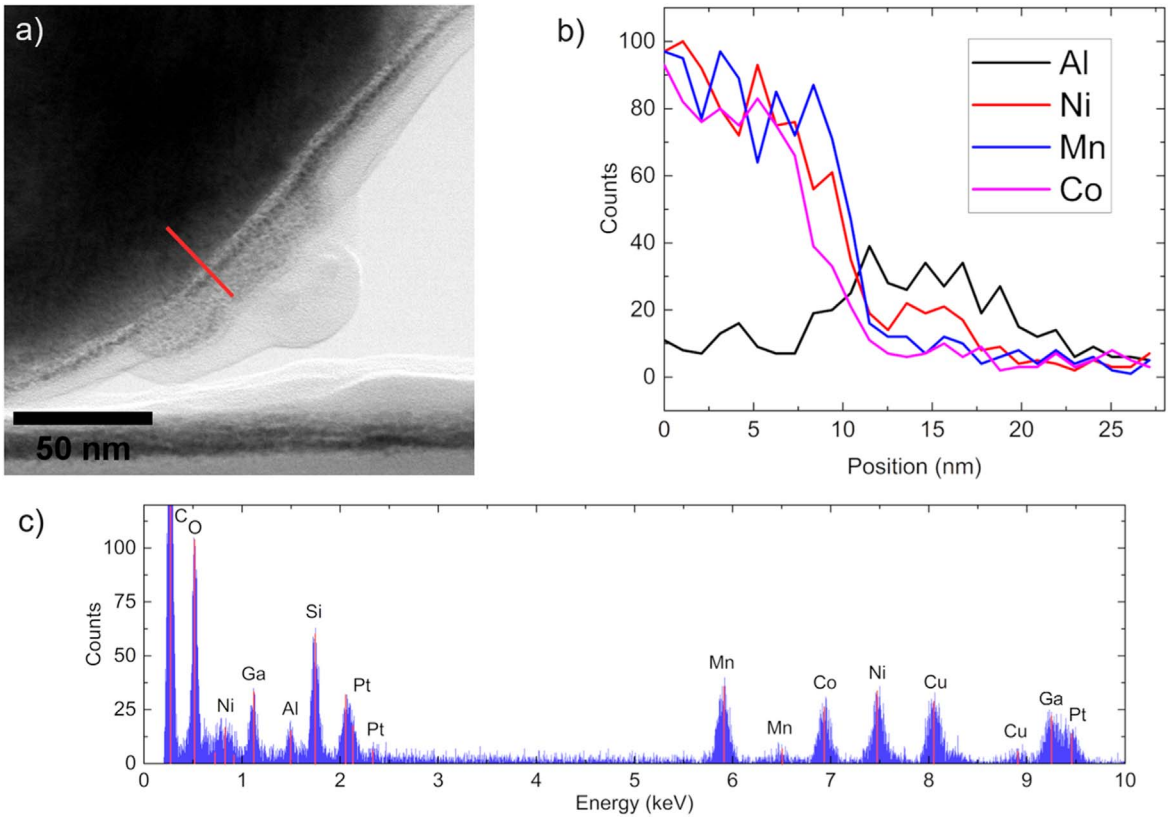

Figure 4. TEM image of coated NCM111 (a), excerpt of EDS line spectrum at the location indicated in image a by the red line (b), cumulative EDS spectrum of the EDS measurements across the red line indicated in image (a) (c).

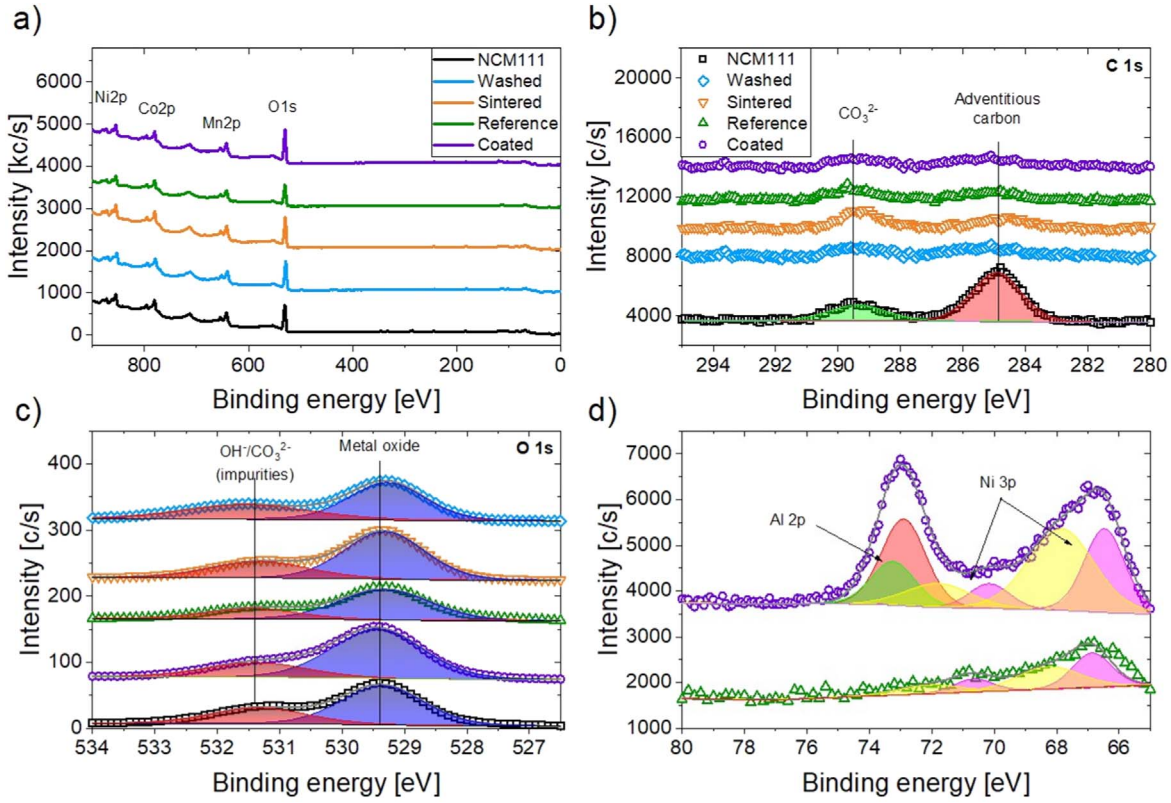

Figure 5. XPS survey (a), Al 2p spectra (b), C 1 s spectra (c), and O 1 s spectra (d) of pristine, reference and coated NCM111. A clearly distinguishable Al 2p peak can be observed at around 73.2 eV for the coated sample.

coated sample also includes signal from the Al_2O_3 coating and is slightly more pronounced comparing to the other samples.

As carbonate impurities on the active material particle surface degrade the battery performance by participating in CEI formation and electrolyte deterioration, estimation of the carbon content in the samples could give an insight into the mechanism of ageing. The carbon XPS spectrum shows two peaks at 284.8 eV and 289.4 eV (Fig. 5b) corresponding to adventitious carbon (hydrocarbons adsorbed on the surface of the particles upon exposure to air) and carbonate impurities, respectively. The adventitious carbon peak is notably more elevated for the pristine NCM111, indicating more adsorbed hydrocarbons on the surface of the unmodified sample. Modifying NCM111 by washing, sintering or both notably decreases the intensity of the adventitious carbon, and the carbonate peak is more prominent than that of the adsorbed carbon in these samples. The coated sample shows the lowest carbonate signal, likely due to $Al_2O_3/LiAlO_2$ covering much of the sample surface. The largest amount of carbonates is observed on the washed samples, as the intensity of the carbonate peak is greater than that of the adventitious carbon. Since washing with ethanol occurs in air and ethanol is hygroscopic, it is possible that some water and other contaminants like CO_2 are pulled into the mixture promoting carbonate formation on sample surface. Significantly lowered carbon content is visible in sintered, reference and coated samples.

The XPS data aligns well with the IRMS results (Fig. 6) which were performed to determine the amount of carbon in the sample. Both pristine and washed samples show the highest carbon content, while sintering reduces the carbon content by approximately half as measured by IRMS. Note that three IRMS measurements were performed for each sample and the error bars in Fig. 6 represent the standard deviation.

ICP-MS analysis was used to quantify the exact concentration of Al in the samples (Fig. S3). The determined content of Al is 0.2 wt% or 0.8 mol%, which means that approximately 10% of the aluminum added in the form of AIP is converted to Al_2O_3 or $LiAlO_2$ after the

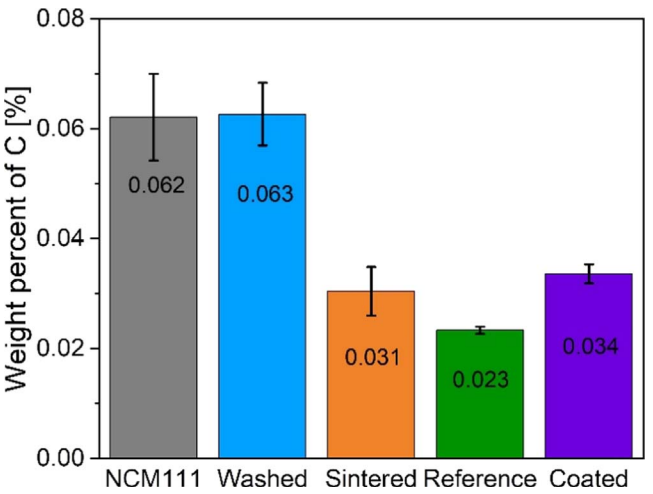

Figure 6. Carbon content in all samples determined by isotope ratio mass spectrometry. A decrease of carbon content in sintered, reference and coated samples is observed in comparison to pristine and washed samples.

synthesis. Interestingly, a slight Mn deficiency was also observed in all NMC materials. After analyzing the amount of Li, Ni, Co and Mn, we conclude that the corresponding stoichiometry is $Li_{1.07}(Ni_{0.36}Co_{0.35}Mn_{0.29})_{0.93}O_2$.

Electrochemical characterization.—All samples display similar charge-discharge voltage profiles (Fig. 7b), while the rate performance (Fig. 7a) suggests small but notable differences in lithium kinetics across the samples. Washing NCM111 appears to have a detrimental and negative effect on the discharge capacity throughout the whole C rate range with the largest drop in capacity being observed at high C rates (5 C, 10 C, and 20 C), indicating slower

electrode kinetics as compared to the pristine NCM111. Sintering has little effect on cell rate capability at any C rate. When the two modification methods, washing and sintering (reference sample), are combined, it appears to have a synergistic effect on the capacity at low C rates (Figs. 7a–7b), however, the rate capability is worse compared to the untreated material. The slower electrode kinetics of the washed sample are also apparent in the reference sample. Considering the variability of the results measured in coin cells,[44] the measured discharge capacities of pristine, sintered, and coated samples may fall within the error range of one another throughout the whole C rate range. However, improved or maintained rate capability has been reported in other coating studies employing $LiAlO_2/Al_2O_3$[17,45–47] despite Al_2O_3 being an isolator. The improved kinetics has been attributed to a decrease in internal resistance observed in impedance studies.

As can be seen from the normalized capacity fade curve (Fig. 7c), the capacity of pristine NCM111 falls to 80% of the initial capacity already within the first 300 cycles, and capacity retention after 500 cycles is around 65%. NCM materials are known to undergo rapid degradation during cycling. The main degradation of NCM111 is localized on the surface and thus the observed capacity fade is mostly due to CEI formation (promoted by surface contamination) and other surface-based degradation mechanisms, as opposed to NCM811 or more Ni-rich NCMs where bulk degradation becomes equally or more severe as the surface degradation.[2,48]

Washing the NCM111 powder with anhydrous ethanol and subsequent drying at 80 °C in vacuum overnight decreases the capacity retention to around 61% after 500 charge-discharge cycles. Although washing in ethanol is reported to partly remove LiOH and other lithium residuals from the surface,[19] some contaminants such as TM carbonates, which notably affect the cycling performance,[4] may remain on the surface and their growth may be further promoted as washing in ethanol includes steps where the cathode material is exposed to ambient air. From the IRMS analysis it was evident that carbon content is not reduced after washing in ethanol, which in combination with the results from XPS (Fig. 5b) suggest that the carbonate content might even be slightly increased. This could at least partly explain the rapid decrease in capacity, since carbonates on the surface of active material particles participate in CEI formation and electrolyte degradation. Note, however, that significant removal of lithium from NCM was not observed by the ICP-MS for any of the samples, and initial Coulombic efficiency of all samples were very similar: 80.6, 83.2, 81.7, 83.0 and 82.7% for pristine, washed, sintered, reference and coated samples respectively. Such results are expected, since washing in ethanol has been shown to dissolve insignificant amounts of Li[19] and sintering can re-insert the Li from surface impurities back into the cathode material.[21]

Sintering the NCM111 powder at 500 °C in air for 4 h improves the capacity retention of the NCM111 material to 76% SoH after 500 cycles. The improvement may be attributed to the removal of surface impurities which can be seen from the reduced amount of C in the sintered sample as measured in the IRMS analysis. Capacity retention could also be improved by regeneration of any surface rock salt phase to layered phase when sintering NCM at high temperatures.[21] Combining the two modification methods (reference sample) produces a capacity fade curve with a capacity retention of 79% - only slightly higher than the capacity retention of the sintered sample. The capacity fade curve of the reference sample is similar to that of the sintered NCM111 half-cell, indicating that the modification step mostly affecting the performance of the reference sample is sintering. The slight increase in capacity retention compared to the sintered sample could be due to slightly lower C content in the reference sample, however, it could also be a result of variation in coin cell preparation.

With a proper reference established, we finally look at the coated sample. Further improvements in capacity retention can be seen for the coated sample (88% after 500 charge-discharge cycles),

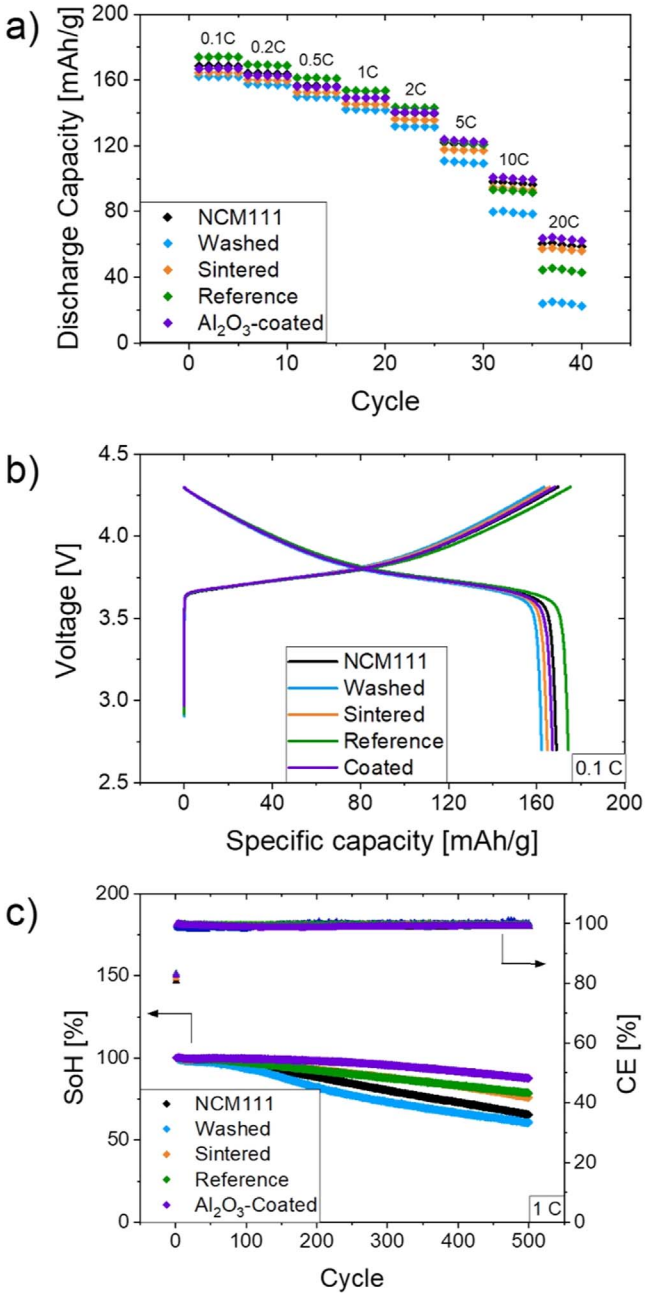

Figure 7. Rate capability measurement (a), charge-discharge curves at 0.1 C (b), SoH evolution during cycling at 1 C (c) for pristine, washed in ethanol, sintered, reference, and coated samples. Charging and discharging were carried out at CC; voltage range for all measurements was 2.7–4.3 V; 1 C = 170 mA g^{-1}.

demonstrating that a protective coating cannot be substituted by simply washing and sintering the material. The coated material exhibits a slightly larger *c*/*a* ratio than pristine and reference samples, indicating an improved 2D character of the material. This is in good agreement with the somewhat improved lithium kinetics. Furthermore, IRMS indicates a lower carbon content on the surface when compared to the pristine sample. The slightly increased carbon content when compared to the reference sample may be due to the coating locking some of the carbon impurities on the particle surface and not allowing them to depart during the sintering step. Nevertheless, these impurities are not directly exposed to the electrolyte, thus, cannot participate in its degradation. The $Al_2O_3/LiAlO_2$ coating can also act as a HF scavenger further

improving the electrochemical stability of the battery cell. All of these factors contribute to a significantly enhanced cycling stability of the coated material.

A drastic improvement can be seen in the capacity retention (65% to 88% SoH after 500 charge-discharge cycles) in our and many other results when comparing the pristine and coated sample. If the experiments are not performed carefully, however, all of the improved cyclability can be falsely attributed to the inert protective coating. However, we have shown here, that some improvement can in fact be attributed to the modification of the active material occurring during the wet-chemical synthesis procedure–especially if the active material has been exposed to air beforehand. In our study, we have shown that after 500 charge-discharge cycles, a pristine, untreated NMC111 cathode material achieves 65% SoH, while the re-sintered sample achieves 79% SoH after the same number of cycles. A significant further cyclability improvement is achieved for the Al_2O_3/$LiAlO_2$-coated samples, achieving 88% SoH after 500 full charge-discharge cycles at 1 C.

Conclusions

A sustainable and non-toxic method to coat NCM111 cathode material with an Al_2O_3-containing coating was developed. The results of this work demonstrate that beyond mimicking the effects of re-sintering, the facile wet-chemical method demonstrated a quantifiable improvement in the cycle life of the Al_2O_3/$LiAlO_2$-coated NCM111 cathode for lithium-ion batteries, with a capacity retention of 88% after 500 charge-discharge cycles, compared to 79% of the reference and 66% of the untreated NCM111 sample.

By carefully analyzing each step of the treatment, we quantify their impact on the electrochemical performance and underline the importance of a proper reference when benchmarking the coated samples. The results show that the capacity retention deteriorates after washing NCM111 in absolute ethanol due to formation of further surface carbonate species. However, subsequent sintering reverses the decreased performance, ultimately enhancing the cycle life compared to the pristine NCM111.

The coated NCM111, which is benchmarked against the re-sintered sample, exhibited excellent capacity retention owing to the maintained layered structure, lower carbon-based impurity content and protective layer which inhibits reactions with the electrolyte and scavenges HF formed during cell operation. Based on the promising results presented in this work, this method provides a pathway towards treating NCM materials to extend their cycle life. In combination with doping and microstructural modification, this method could be used to extend the cycle life of NCMs with higher Ni content and successfully mitigate surface-based degradation.

Acknowledgments

The support of the M-Era.net project “Inert Coatings for Prevention of Ageing of NMC Cathode for Lithium-Ion Batteries” (InCoatBat), Project Reference Number 10341 is acknowledged. Institute of Solid-State Physics, University of Latvia as the Centre of Excellence has received funding from the European Union’s Horizon 2020 Framework Program H2020-WIDESPREAD-01–-2016–2017-TeamingPhase2 under grant agreement No. 739508, project CAMART2.

ORCID

Gints Kucinskis https://orcid.org/0000-0001-9432-2358

References

1. A. Alessia, B. Alessandro, V. G. Maria, V. A. Carlos, and B. Francesca, *J. Clean. Prod.*, **300**, 126954 (2021).
2. H. J. Noh, S. Youn, C. S. Yoon, and Y. K. Sun, *J. Power Sources*, **233**, 121 (2013).
3. L. Britala, M. Marinaro, and G. Kucinskis, *J Energy Storage*, **73**, 108875 (2023).
4. J. Sicklinger, M. Metzger, H. Beyer, D. Pritzl, and H. A. Gasteiger, *J. Electrochem. Soc.*, **166**, A2322 (2019).
5. P. Teichert, G. G. Eshetu, H. Jahnke, and E. Figgemeier, *Batteries*, **6**, 8 (2020), https://mdpi.com/2313-0105/6/1/8/htm.
6. H. Zhang, J. Xu, and J. Zhang, *Front Mater*, **6**, 504473 (2019).
7. X. Xiong et al., *J. Solid State Electrochem.*, **18**, 2619 (2014).
8. S. She, Y. Zhou, Z. Hong, Y. Huang, and Y. Wu, *ACS Omega*, **7**, 24851 (2022).
9. M. Park, X. Zhang, M. Chung, G. B. Less, and A. M. Sastry, *J. Power Sources*, **195**, 7904 (2010).
10. X. Li et al., *RSC Adv.*, **7**, 24359 (2017), https://pubs.rsc.org/en/content/articlehtml/2017/ra/c7ra03438e.
11. B. Li et al., *ChemistrySelect*, **4**, 6354 (2019).
12. J. Zhu et al., *J. Alloys Compd.*, **773**, 112 (2019).
13. X. Xiong, Z. Wang, X. Yin, H. Guo, and X. Li, *Mater. Lett.*, **110**, 4 (2013).
14. Y. Huang, F. M. Jin, F. J. Chen, and L. Chen, *J. Power Sources*, **256**, 1 (2014).
15. B. Han et al., *ACS Appl. Mater. Interfaces*, **9**, 14769 (2017).
16. G. Kaur and B. D. Gates, *J. Electrochem. Soc.*, **169**, 043504 (2022).
17. R. S. Negi and M. T. Elm, *Scientific Data*, **9**, 1 (2022), https://nature.com/articles/s41597-022-01217-5.
18. D. Hu et al., *J. Electroanal. Chem.*, **880**, 114910 (2021).
19. Y. Zhou, Z. Hu, Y. Huang, Y. Wu, and Z. Hong, *J. Alloys Compd.*, **888**, 161584 (2021).
20. W.-min Liu et al., *Transactions of Nonferrous Metals Society of China*, **28**, 1626 (2018).
21. B. Huang et al., *ACS Appl. Mater. Interfaces*, **11**, 14076 (2019).
22. X. Xiong et al., *J. Power Sources*, **222**, 318 (2013).
23. Y. Su et al., *Front Chem*, **8**, 573 (2020).
24. C. Busà, M. Belekoukia, and M. J. Loveridge, *Electrochim. Acta*, **366**, 137358 (2021).
25. H. S. Liu, Z. R. Zhang, Z. L. Gong, and Y. Yang, *Electrochem. Solid-State Lett.*, **7** (2004).
26. H. Choi, A. R. Schuer, H. Moon, M. Kuenzel, and S. Passerini, *Electrochim. Acta*, **430**, 141047 (2022).
27. I. Hwang, C. W. Lee, J. C. Kim, and S. Yoon, *Mater. Res. Bull.*, **47**, 73 (2012).
28. J. Zhang, J. Qiao, K. Sun, and Z. Wang, *Particuology*, **61**, 18 (2022).
29. L. Fernandez-Diaz et al., *Chem. Eng. J.*, **464**, 142469 (2023).
30. A. Ponrouch and M. R. Palacín, *J. Power Sources*, **196**, 9682 (2011).
31. W. Hua et al., *J. Electrochem. Soc.*, **166**, A5025 (2019), https://iopscience.iop.org/article/10.1149/2.0051903jes.
32. A. O. Kondrakov et al., *J. Phys. Chem. C*, **121**, 3286 (2017).
33. Y. Bentaleb et al., *J. Power Sources*, **195**, 1510 (2010).
34. B. Han et al., *ACS Appl. Mater. Interfaces*, **9**, 41291 (2017).
35. S. Buta, D. Morgan, A. Van der Ven, M. K. Aydinol, and G. Ceder, *J. Electrochem. Soc.*, **146**, 4335 (1999).
36. H. Zhang and J. Zhang, *eTransportation*, **7**, 100105 (2021).
37. L. Noerochim, S. Suwarno, N. H. Idris, and H. K. Dipojono, *Batteries*, **7**, 84 (2021), https://mdpi.com/2313-0105/7/4/84/htm.
38. J. Zhou, X. Zhou, W. Yu, Z. Shang, and S. Xu, *Electrochemical Energy Reviews*, **7**, 1 (2024).
39. R. S. Negi et al., *Adv. Mater. Interfaces*, **9**, 2101428 (2022).
40. O. Touag et al., *Energy Advances*, **2**, 701 (2023), https://pubs.rsc.org/en/content/articlehtml/2023/ya/d3ya00061c.
41. J. L. White, F. S. Gittleson, M. Homer, and F. El Gabaly, *J. Phys. Chem. C*, **124**, 16508 (2020).
42. R. Li et al., *RSC Adv.*, **9**, 36849 (2019), https://pubs.rsc.org/en/content/articlehtml/2019/ra/c9ra07873h.
43. X. Ren et al., *Ionics (Kiel)*, **26**, 1617 (2020).
44. A. Smith et al., *Batter Supercaps*, **6**, e202300080 (2023).
45. J. Cho, Y. J. Kim, and B. Park, *Chem. Mater.*, **12**, 3788 (2000).
46. R. S. Negi, S. P. Culver, A. Mazilkin, T. Brezesinski, and M. T. Elm, *ACS Appl. Mater. Interfaces*, **12**, 31392 (2020).
47. A. Zhou et al., *J Mater Chem A Mater*, **5**, 24361 (2017).
48. H. H. Ryu, K. J. Park, C. S. Yoon, and Y. K. Sun, *Chem. Mater.*, **30**, 1155 (2018).